

Spatio-Contextual Deep Network Based Multimodal Pedestrian Detection For Autonomous Driving

Kinjal Dasgupta¹, Arindam Das², Sudip Das¹, Ujjwal Bhattacharya¹ and Senthil Yogamani³

Abstract—Pedestrian Detection is the most critical module of an Autonomous Driving system. Although a camera is commonly used for this purpose, its quality degrades severely in low-light night time driving scenarios. On the other hand, the quality of a thermal camera image remains unaffected in similar conditions. This paper proposes an end-to-end multimodal fusion model for pedestrian detection using RGB and thermal images. Its novel spatio-contextual deep network architecture is capable of exploiting the multimodal input efficiently. It consists of two distinct deformable ResNeXt-50 encoders for feature extraction from the two modalities. Fusion of these two encoded features takes place inside a multimodal feature embedding module (MuFEM) consisting of several groups of a pair of Graph Attention Network and a feature fusion unit. The output of the last feature fusion unit of MuFEM is subsequently passed to two CRFs for their spatial refinement. Further enhancement of the features is achieved by applying channel-wise attention and extraction of contextual information with the help of four RNNs traversing in four different directions. Finally, these feature maps are used by a single-stage decoder to generate the bounding box of each pedestrian and the score map. We have performed extensive experiments of the proposed framework on three publicly available multimodal pedestrian detection benchmark datasets, namely KAIST, CVC-14, and UTokyo. The results on each of them improved the respective state-of-the-art performance. A short video giving an overview of this work along with its qualitative results can be seen at <https://youtu.be/FDjSifuuCs>.

Index Terms—Pedestrian Detection, Multi-spectral Imagery, Thermal Imagery, Multimodal Feature Fusion, Deep Learning.

I. INTRODUCTION

Object detection is an extensively studied area of Computer Vision, while pedestrian detection is a special case of the same. There are several important applications of automatic pedestrian detection, and the most significant one is autonomous driving. Cameras are the primary sensor as the transportation infrastructure is built for human optical sensing and also because of the dense semantic and geometric information it captures at low cost. Due to the safety requirements of an autonomous driving system, multiple sensors, including camera, lidar, radar, ultrasonic, etc., are commonly used to improve reliability and safety. There is extensive research performed on pedestrian detection [1]. The majority of pedestrian detection studies [2] considered images captured by RGB cameras under daylight conditions. One of the main challenges is its performance in adverse weather and poor lighting conditions. In particular, night time scenarios with illuminance

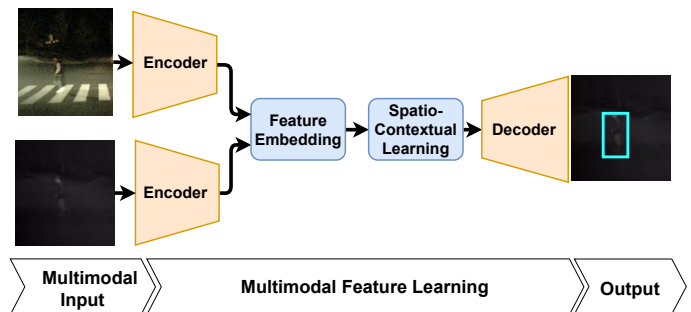


Fig. 1: Our **multimodal pedestrian detection model** consists of two unimodal encoders and a single-stage detection decoder. We design two novel modules for efficient feature embedding and spatio-contextual feature representation learning.

levels less than 1 lux have poor performance. The quality of semantic representation of the object can degrade severely with insufficient lighting. A large proportion of pedestrian-related accidents occurs in the night time in the case of human driving [3]. Thus it is necessary to achieve robust pedestrian detection at night time in an autonomous driving system. This is achieved by making use of multiple complementary sensors and using fusion algorithms to improve the reliability [4], [5].

The infrared spectrum lies below the visible spectrum used by RGB cameras. It is categorized into near and far-infrared regions with a region in the middle, further sub-divided into short, mid, and long wavelengths. Mid and long-wavelength infrared are commonly known as thermal infrared as the intensity of captured radiation are correlated with the temperature of an object [6]. They are typically passive sensors compared to near-infrared sensors, which require an active source to illuminate the scene. Passive sensors are cost-effective and beginning to be a crucial sensor for autonomous driving. They are commonly used in automotive night vision systems providing a display on the dashboard monitor. Toyota was one of the first to deploy it in 2002 in the Land-Cruiser vehicle. Audi A8 and BMW 7 series released thermal camera-based night vision systems with animal detection feature [7]. More recent systems support pedestrian detection and animal detection as they have unique thermal signatures relative to other objects. Thermal sensors are also robust in bright sun glare scenarios, which is another major challenge in automated driving [8].

In this paper, we propose an end-to-end CNN based fusion model for pedestrian detection using both thermal and RGB images as illustrated in Figure 1. Thermal cameras are less variant to ambient light and capture less texture compared to

¹CVPR Unit, Indian Statistical Institute, Kolkata, India.

²Detection Vision Systems, Valeo India.

³Valeo Visions Systems, Ireland.

Corresponding Email: arindam.das@valeo.com

RGB cameras. Thus there is a significant domain gap between them, and an effective fusion strategy is necessary. We use a standard encoder to perform unimodal feature extraction independently for the two input modalities. We propose a multimodal feature embedding module using graph attention network and spatio-contextual feature aggregation module using channel attention and multi-directional RNN to obtain multimodal features. Finally, the multimodal features are input to a single stage detection decoder which produces pedestrian bounding boxes and score maps.

The main contributions of our work include the:

- 1) Design of a novel multimodal feature embedding module using graph attention network and feature fusion unit to address the modality imbalance problem.
- 2) Design of a spatio-contextual feature aggregation module to improve fusion using CRF-based refinement, channel-wise attention, and 4Dir-IRNN components.
- 3) Implementation of an end-to-end trainable network achieving state-of-the-art results on three public datasets, namely KAIST, CVC-14, and UTokyo.
- 4) Extensive experimentation of different feature encoders, network components, various augmentation strategies, curriculum learning, and tuning of hyper-parameters.

II. RELATED WORK

Usage of thermal imagery for pedestrian detection has received significant interest due to the increasing availability of low-cost thermal sensors. In this section, we first briefly discuss the pedestrian detection literature on visible and thermal sensors. Then we discuss multimodal pedestrian detection based on the fusion of both sensors, which is the focus of this work. We use the more generic term *multimodal* instead of the specific term *multispectral* which refers to thermal and image belong to different spectra.

A. Visible spectrum based pedestrian detection

Adverse weather conditions such as fog, rain, dust, varied illumination, complex background make the pedestrian detection task extremely difficult in the visible spectrum. To solve such issues to some extent, a joint optimization approach was proposed in [9] where semantic attributes were learned for pedestrian detection along with scene attributes. Similar approaches are observed in [10], [11] where other vision tasks are added to influence pedestrian detection. In another study [12], generic Faster-RCNN [13] was adapted to solve the problem of pedestrian detection. One of the recent works [14] proposed an anchor-free method for pedestrian detection.

B. Thermal imagery-based pedestrian detection

Relatively, there is limited literature on pedestrian detection solely based on thermal imagery. Baek et al. [15] proposed a detection method specific to nighttime only by leveraging thermal-position-intensity-histogram of oriented gradients (T π HOG) combined with the additive kernel SVM (AKSVM). The method in [16] used thermal images along with saliency

maps as part of augmentation. The intention to use this map is to employ an attention mechanism in the network to train Faster R-CNN [13]. A “pseudo-multimodal” object detector was proposed in [17] where pseudo-RGB equivalent images were generated using Cycle-GAN [18] based image-to-image translation framework. Recently, domain adaptation has been applied in [19], [20] for pedestrian detection to leverage existing camera datasets.

C. Multimodal pedestrian detection

Fusion of both the visible spectrum and thermal images has been proven to be effective in the recent literature [21], [22], [23], [24]. Yadav et al. [25] used a simple fusion strategy and showed good performance for multimodal pedestrian detection. An extensive study of various fusion architectures was explored in [22]. Four different network fusion methods (early, halfway, late, and score fusion) of both visible and thermal data were studied for multimodal pedestrian detection. The halfway fusion model achieved the best detection performance, and we adopt the same fusion strategy. Most of the well-performing multimodal pedestrian detection networks are built upon both variants of R-CNNs. The authors in [26] proposed illumination aware Faster R-CNNs to perform multimodal pedestrian detection. Two Single Shot Detectors (SSDs) were employed in [27] to effectively fuse the features from the visible spectrum and thermal using Gated Fusion Units. Zhang et al. [28] highlighted the position shift problem in color-thermal image pairs. This shift in the data for one modality affects another as they are not aligned. The possible reasons for this shift are hardware aging, a shift in field-of-view of two modalities, different resolutions, issues in alignment algorithm, etc. Zhou et al. [29] addressed the modality imbalance problem for multimodal data and presented an in-depth study on the efficient fusion of two modalities.

III. PROPOSED METHOD

The overall architecture of the proposed method is illustrated in Figure 2. We use ResNeXt-50 [33] backbone using Deformable Convolution Network (DCN) [30] to obtain feature extraction independently for both the modalities. The two unimodal encoder feature maps are combined in *Multimodal Feature Embedding Block (MuFEm)* and further refined in *Spatio-Contextual Feature Aggregation Block (SCoFA)* to combine the complementary information from the two sensors effectively. Finally, a single stage detection decoder [34] uses the multimodal features to output bounding boxes and scores for pedestrians. We discuss these components in detail in the following sub-sections.

A. Unimodal Feature Encoders

Pedestrians are articulated objects undergoing non-rigid motion. In addition, they suffer from self-occlusion in crowded areas and occlusion due to blockage by other objects. Thus, we are motivated to use deformable convolution, which can handle these geometric deformations better. Deformable convolutions were first introduced in [30] to have an adaptation mechanism

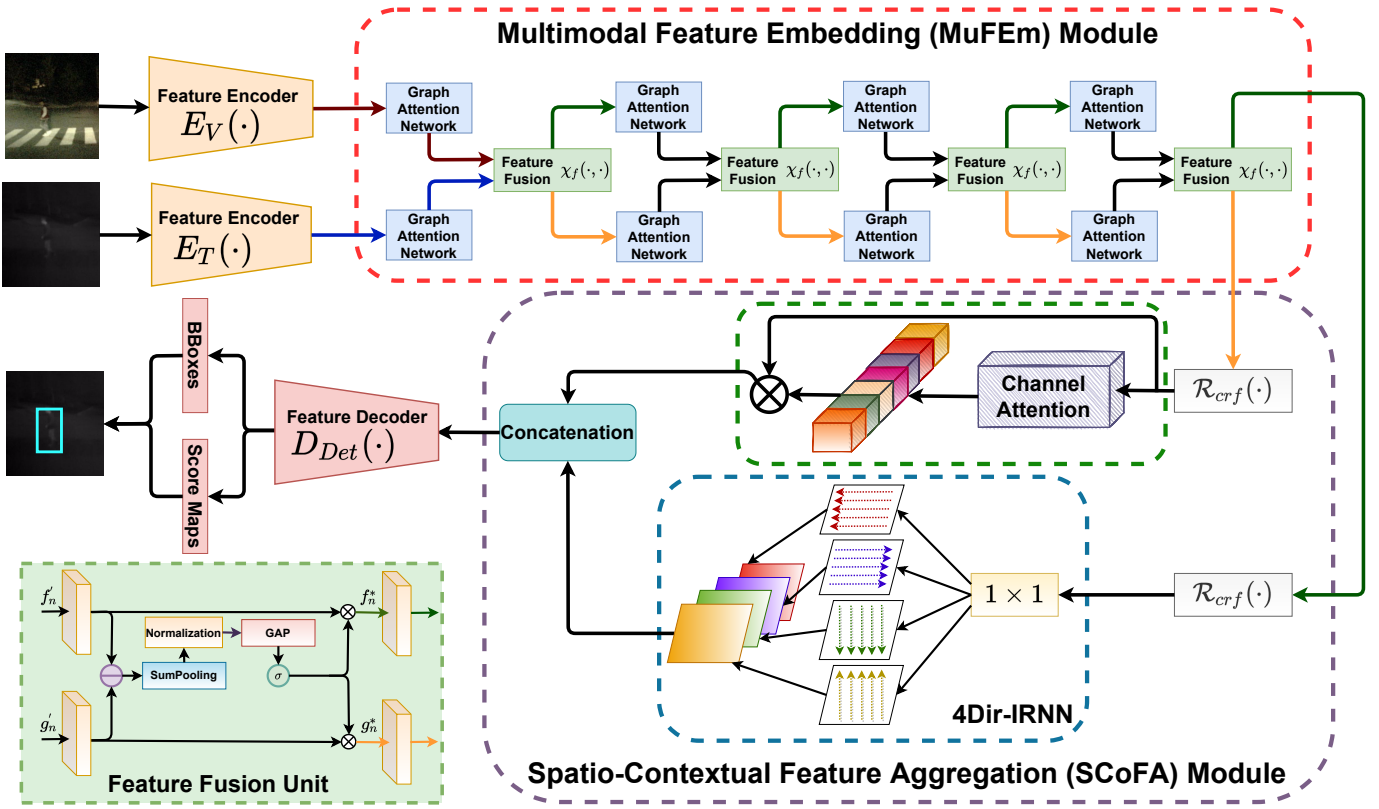


Fig. 2: **Our proposed architecture for end-to-end multimodal pedestrian detection.** The input RGB & thermal images are passed through two separate deformable ResNext-50 [30] based feature encoders $E_V(\cdot)$ & $E_T(\cdot)$ respectively. The outputs from these encoders are passed through a *Multimodal Feature Embedding (MuFEM) Module* consisting of multiple instances of *Graph Attention Network* [31] and *Feature Fusion Unit* $\chi_f(\cdot, \cdot)$. The two outputs of MuFEM are fed to two distinct CRF based *Feature Aggregation Units* $\mathcal{R}_{crf}(\cdot)$ which belong to a *Spatio-Contextual Feature Aggregation (SCoFA) Module*. The *SCoFA* module additionally contains a channel-wise attention and 4Dir-IRNN component [32] each of which receives input from one of the two $\mathcal{R}_{crf}(\cdot)$. The outputs of these 2 components are concatenated & passed to the feature decoder $D_{Det}(\cdot)$ with several deconvolutional layers. The final outputs of $D_{Det}(\cdot)$ consist of a Score Map & bounding boxes.

in the convolution showing significant improvements over the traditional convolution. FisheyeDistanceNet [35] successfully made use of it to handle the spatially varying radial distortion. In this work, we use DCN to learn better the appearance of pedestrians with geometric and lighting condition variations. Deformable convolution [30] has two parts: a regular convolution layer and a deformable grid with a learnable 2D offset. Grid is adapted based on data, and the convolution layer is applied on the deformed grid. The generalized convolution combining these two operations is shown below.

$$\mathcal{Y}(\mathcal{P}_0) = \sum_{\mathcal{P}_i \in \mathcal{C}} \mathcal{W}(\mathcal{P}_i) \odot \mathcal{X}(\mathcal{P}_0 + \mathcal{P}_i + \Delta\mathcal{P}_i) \quad (1)$$

where \mathcal{P}_0 is the center of the grid, and \mathcal{P}_i is the point that iterates over the set \mathcal{C} of the sampling points in the grid. Thus the sampling can be irregular and offset locations $\mathcal{P}_i + \Delta\mathcal{P}_i$, i.e., sampling locations of the kernel are redistributed with the new shapes which may not be rectangular.

B. Multimodal Feature Embedding Block (MuFEM)

MuFEM uses the unimodal encoder features as the input and outputs multimodal features. It consists of two parallel blocks of Graph Attention Networks (GAT) [31] where the outputs are further fused in the Feature Fusion Unit. This basic unit is

repeated several times to obtain progressively aligned feature maps. The details of the GAT and Feature Fusion Unit are discussed in detail below.

1) *Graph Attention Network*: Graph Attention Network (GAT) [31] was formulated to work on graph data structures using self-attention layers. Their formulation also enabled easy stacking of several GAT layers. In our case, the feature maps are on a dense grid which is a special case of a graph, but it has a very regular structure. There is little work on using graph convolutions for a dense grid. Gao et al. [36] extended semantic segmentation using graph convolutions. Cai et al [37] successfully applied graph convolutions with cross-attention for remote sensing image classification. We are motivated to use GAT to better handle pixel misalignment across the sensors and non-rigid transformations of pedestrians.

GAT layer uses a graph and its adjacency matrix as the input. We propose to divide the feature map grid structure $\mathcal{F}_n \in \mathbb{R}^{H \times W \times C}$ into several local feature maps $h = \{h_1, h_2, \dots, h_N\}$, $h_i \in \mathbb{R}^{\mathcal{F}}$ where N is the node of the graph and \mathcal{F} represents the number of features in each node. Every node of this graph network is fully connected to each other. Each connection between two nodes captures the relationship between the local features. A new set of node features $h = \{h_1^{\vec{h}}, h_2^{\vec{h}}, \dots, h_N^{\vec{h}}\}$, $h_i^{\vec{h}} \in \mathbb{R}^{\mathcal{F}'}$ is obtained as its output by sharing the information between the adjacency matrix of

the previous graph layer nodes and the local features. A max pooling operation is performed on each extracted local features $\vec{h}_i \in \mathbb{R}^{\mathcal{F}} \forall i$. Then a transformation weight matrix which is linear in nature $\mathcal{W} \in \mathbb{R}^{\mathcal{F} \times \mathcal{F}'}$ is applied on each channel to obtain a global feature representation from \vec{h}_i . It is followed by a shared self-attention mechanism $a: \mathbb{R}^{\mathcal{F} \times \mathcal{F}'} \rightarrow \mathbb{R}$ defined in Equation 2.

$$e_{ij} = a(\mathcal{W}\vec{h}_i, \mathcal{W}\vec{h}_j) \quad (2)$$

where i and j are two nodes of a graph and e_{ij} is the attention coefficient that captures the information exchange between i th and j th node. We normalize the function using softmax function in Equation 3 to make the coefficients comparable across different nodes.

$$\alpha_{ij} = \frac{\exp(e_{ij})}{\sum_{k \in \mathcal{N}_i} \exp(ik)} \quad (3)$$

where \mathcal{N}_i is the size of the graph where all the nodes are connected to each other.

Finally, an attention mechanism based on a feed-forward neural network has been applied, parameterized using a weight vector $\vec{a} \in \mathbb{R}^{2 \times \mathcal{F}'}$ and employing the LeakyReLU non-linearity ($\alpha = 0.2$) as shown in the equation below.

$$\alpha_{ij} = \frac{\exp\left(\text{LeakyReLU}(\vec{a}^T)[\mathcal{W}\vec{h}_i \parallel \mathcal{W}\vec{h}_j]\right)}{\sum_{k \in \mathcal{N}_i} \exp\left(\text{LeakyReLU}(\vec{a}^T)[\mathcal{W}\vec{h}_i \parallel \mathcal{W}\vec{h}_j]\right)} \quad (4)$$

2) *Feature Fusion Unit ($\mathcal{X}_f(\cdot)$):* The unimodal features modulated by Graph Convolution Network (GAT) are then fed to the Feature Fusion Unit $\mathcal{X}_f(\cdot)$. It is designed to enable an effective combination of the unimodal features with the domain gap, mainly based on illumination. It is illustrated in the bottom left corner of Figure 2.

The Feature Fusion unit receives two sets of input feature f'_n and g'_n from the two distinct GAT modules. These two sets of feature maps are from two different modalities. We aim to convert the modality-specific features to a modality invariant feature representation for efficient feature embedding reducing the domain gap in feature space. To accomplish this, we subtract the features coming from two different modalities and use them to guide the normalization. Then we feed it into the Global Average Pooling (GAP) layer and apply the *tanh* activation function to obtain modality agnostic feature representation. Finally, the f'_n and g'_n are re-calibrated by channel-wise multiplication of domain invariant features obtained. We do this iteratively in stages during the course of training that helps to minimize the domain gap and generates domain invariant features for pedestrians.

C. Spatio-Contextual Feature Aggregation Block (SCoFA)

Spatio-Contextual Feature Aggregation Block (SCoFA) module consists of two blocks. First, a Conditional Random Fields (CRFs) based aggregation block $\mathcal{R}_{crf}(\cdot)$ followed by channel-wise attention is used to extract the spatial features of the pedestrians. Then, a four-directional IRNN architecture (4Dir-IRNN) block [32] is used to extract the contextual features of the pedestrians. IRNN is a Recurrent Neural

Network (RNN) whose weight matrix is initialized by an Identity matrix.

Liu et al. [38] introduced a deep structured model using CRFs to refine CNN features using a message passing mechanism for the crowd counting problem. Inspired by this work, we make use of the $\mathcal{R}_{crf}(\cdot)$ block to obtain robust and refined features, particularly for crowded pedestrian scenes. There are two distinct $\mathcal{R}_{crf}(\cdot)$ blocks which independently process the two set of feature maps output from *MuFEm* block. Automotive scenes have a strong context and prior geometry to be exploited. There is a structured roadway for vehicles and a sidewalk for pedestrians. Bell et al [32] designed a 4Dir-IRNN to extract context features for object detection in MS COCO dataset. We adapt the 4Dir-IRNN in our proposed architecture to exploit the road scene geometry. Context features can also aid detections in case of occlusions or poor visibility.

In order not to degrade spatial features, we have a parallel $\mathcal{R}_{crf}(\cdot)$ block, which is fed to a channel attention block which is finally concatenated with the context features. The channel-wise attention is used for enhancing inter-channel relationships. Furthermore, it alleviates the removal of unwanted background information and noise in the feature maps from $F_{R_{crf}}$. It is represented by the function below.

$$\mathcal{F}_{att} = \mathcal{F}_{R_{crf}} \otimes \sigma(\text{Conv}_{1 \times 1}(\mathcal{F}_{R_{crf}})) \quad (5)$$

Each instance of RNN consumes a sequence of 512 channels of the input feature map after being processed by a $\text{Conv}_{1 \times 1}$ block. 4Dir-IRNN traverses in four directions (right to the left, left to right, top to bottom, and bottom to top) illustrated in Figure 2 to obtain context features. Furthermore, the contextual features obtained from the multi-directional RNNs are directly concatenated to produce \mathcal{F}_{IRNN} which is further concatenated to \mathcal{F}_{att} to obtain the final feature vector.

D. Feature Decoder Block & Detection Branch

We design a single-stage detection decoder $\mathcal{D}_{Det}(\cdot)$ which uses the feature maps from the *SCoFA* as input and outputs bounding boxes with score maps.

We adapt the EAST decoder [34] designed for efficient text detection. We progressively upsampled the previous layer by 2 and reduced the number of channels from 256 to 32 before feeding into the detection branch. Then it is passed through four $\text{Conv}_{1 \times 1}$ layers that produce 4 channels of feature maps. The final layer regresses the score map and rotated boxes. The loss function of detector is provided in Equation 6.

$$\mathcal{L} = \mathcal{L}_s + \lambda_g \mathcal{L}_g, \quad (6)$$

where \mathcal{L}_s and \mathcal{L}_g correspond to the loss of the Score Map and geometric loss of rotated box, respectively, λ_g represents the weighting ratio between the two losses.

Bounding box is represented by the top left and right bottom ends represented in the output coordinate grid as $p_t = (x_t, y_t)$ and $p_b = (x_b, y_b)$. For every pixel, the output feature map consists of a bounding box and a detection score. We use the class balanced cross-entropy loss [41] in score map prediction as shown in Equation 7.

Encoders	Number of Fusion Units					Feature Aggregation			Miss Rate		
	1	2	3	4	5	Spatial	Contextual	Both	All	Day	Night
ResNet-50 [39]	✓	✗	✗	✗	✗	✓	✗	✗	26.23	27.35	25.67
	✓	✗	✗	✗	✗	✗	✓	✗	25.01	25.17	24.45
	✓	✗	✗	✗	✗	✗	✗	✓	23.98	24.66	22.01
	✗	✓	✗	✗	✗	✓	✗	✗	23.53	23.62	21.97
	✗	✓	✗	✗	✗	✗	✓	✗	22.31	23.99	20.78
	✗	✓	✗	✗	✗	✗	✗	✓	20.87	20.96	19.31
	✗	✗	✓	✗	✗	✓	✗	✗	21.83	21.97	21.27
	✗	✗	✓	✗	✗	✗	✓	✗	20.61	20.74	20.05
	✗	✗	✓	✗	✗	✗	✗	✓	18.17	19.26	19.11
	✗	✗	✗	✓	✗	✓	✗	✗	19.13	19.22	18.57
	✗	✗	✗	✓	✗	✗	✓	✗	18.91	19.17	18.35
	✗	✗	✗	✓	✗	✗	✗	✓	15.47	16.56	15.91
	✗	✗	✗	✗	✓	✓	✗	✗	19.09	19.2	18.35
	✗	✗	✗	✗	✓	✗	✓	✗	18.78	19.12	18.16
	✗	✗	✗	✗	✓	✗	✗	✓	15.26	16.44	16.21
	✓	✗	✗	✗	✗	✓	✗	✗	20.53	20.62	19.97
	✓	✗	✗	✗	✗	✗	✓	✗	18.76	19.08	19.64
	✓	✗	✗	✗	✗	✗	✗	✓	17.87	18.96	17.31
	✗	✓	✗	✗	✗	✓	✗	✗	16.02	17.11	16.46
	✗	✓	✗	✗	✗	✗	✓	✗	15.88	16.97	16.22
	✗	✓	✗	✗	✗	✗	✗	✓	13.67	15.76	14.11
	✗	✗	✓	✗	✗	✓	✗	✗	13.62	14.73	14.66
	✗	✗	✓	✗	✗	✗	✓	✗	11.48	13.03	12.8
	✗	✗	✓	✗	✗	✗	✗	✓	10.27	11.96	11.41
✗	✗	✗	✓	✗	✓	✗	✗	11.52	12.87	11.92	
✗	✗	✗	✓	✗	✗	✓	✗	10.38	10.49	9.93	
✗	✗	✗	✓	✗	✗	✗	✓	9.23	9.33	8.97	
✗	✗	✗	✗	✓	✓	✗	✗	11.56	12.67	12.03	
✗	✗	✗	✗	✓	✗	✓	✗	10.45	10.57	10.0	
✗	✗	✗	✗	✓	✗	✗	✓	9.39	9.74	9.06	

TABLE I: Ablation study of the proposed architecture on KAIST dataset [40]. *MuFEm* module consists of several cascaded blocks of Graph Attention Network [31] & a Feature Fusion Unit. Ablation study is conducted on spatial (channel wise attention) & contextual (4Dir-IRNN [32]) feature branch of *SCoFA* modules varying the number of Fusion Units from 1 to 5.

IV. EXPERIMENTATION DETAILS

$$\mathcal{L}_s = -\beta S^{GT} \log S^P - (1 - \beta)(1 - S^{GT}) \log(1 - S^P) \quad (7)$$

where S^P is the prediction of the score map and S^{GT} is ground truth. It is to be noted that β plays the role of class balancing weight factor between positive and negative input samples.

The sizes of pedestrians vary widely and it is a main challenge in the pedestrian detection problem. Regression loss using $L1$ or $L2$ may give more importance to larger sized bounding boxes and a scale-invariant loss is more suitable. Thus we chose to use the IoU loss [34] for the Bounding Box (BBox) regression as shown below.

$$\begin{aligned} \mathcal{L}_g &= -\log \text{IoU}(BBox^P, BBox^{GT}) \\ &= -\log \frac{|BBox^P \cap BBox^{GT}|}{|BBox^P \cup BBox^{GT}|} \end{aligned} \quad (8)$$

where $BBox^P$ is the predicted bounding boxes of the pedestrians while $BBox^{GT}$ represents the ground truth of the corresponding pedestrians.

A. Dataset and evaluation metrics

In this work, we make use of the following three main publicly available multimodal datasets discussed below.

KAIST: KAIST [40] is the commonly used dataset for Multimodal Pedestrian Detection. It consists of 95,000 *color-thermal* pairs of frames with 103,128 annotated bounding box and 1,182 distinct pedestrians. The frames were captured in both day and night time scenarios and it contains more granular annotations such as sunrise, morning, afternoon, sunset, night, and dawn. The dataset contains pedestrians with many partially occluded and heavily occluded instances. Alignment issues in the original dataset were fixed by Zhang et al. [28] and test annotations were refined by Liu et al. [22]. We use the latest version of the dataset with these fixes.

CVC-14: The CVC-14 dataset [42] contains video sequences of *grayscale-thermal* pair captured at 10 FPS during day and night time. The sample distribution for training and testing in the dataset follows 7,085 and 1,433 frames, respec-

tively. Annotations for each modality are provided individually as the camera extrinsic was not calibrated properly.

UTokyo: The UTokyo multimodal dataset [43] contains a total of 7,512 images captured during day (3,740) and night (3,772) time at 1 FPS in a university campus using RGB, far-infrared (FIR), mid-infrared (MIR), and near-infrared (NIR) cameras. In this work, we only use the samples that are aligned to enable comparison with other methods.

For detection accuracy of the pedestrians, we use the standard log average Miss Rate (MR) to calculate the error. We also use mAP (mean average precision) to compare with few other works. Note that higher mAP is better, whereas lower MR is better. All methods reported in this work are evaluated based on the standard protocol called *reasonable* setup [44] for KAIST dataset [40] where pedestrian boxes are over 50 pixels tall under no or partial occlusion.

B. Ablation study

We chose KAIST [40] for our ablation studies as it is the largest and the most commonly used dataset for multimodal pedestrian detection. Thus, we perform a broad range of systematic experiments as part of the ablation study on this dataset to find the optimal configuration of our model. The network is trained using Momentum Optimizer with an initial learning rate of 0.01 and momentum set to 0.9. A factor of 10 then reduces the learning rate after the completion of every 5k iterations. The proposed model was trained on a system with two Nvidia Tesla P6 GPUs, and the batch size was set to 1.

Network components: The basic fusion unit in *MuFEM* module consists of a pair of Graph Attention Networks (GATs) operating parallelly, and a feature fusion unit combines their outputs. We repeat these blocks to combine the unimodal feature maps progressively. We vary the number of fusion units from 1 to 5. For each of these configurations, we do ablation of the spatial and contextual components of the *SCoFA* module. Experiments are performed with both these enabled together and with only one of them enabled. To keep the size of the network reasonable, we make use of ResNet-50 [39] as the baseline instead of ResNet-101. We also used ResNeXt-50 [33] encoder which is an improvement over ResNet. Both these encoders used deformable convolution [30] as our initial set of experiments demonstrate a significant improvement over regular convolutions. Thus we made an early design choice to use DCN and we did not perform ablation study on this with other network components to limit the number of combinations.

Table I summarizes the ablation study of network architecture components. Accuracy increases progressively with number of fusion units and saturates at 4. Spatial and contextual blocks in *SCoFA* provide a significant improvement on top of optimal *MuFEM* setting. The best setting is for usage of both spatial and contextual blocks in *SCoFA* and 4 fusion units in *MuFEM* with ResNeXt-50 encoder. All the further experiments make use of this configuration.

Curriculum Learning: Curriculum Learning [45] is a training method that aims to gradually increase the complexity of the data fed to the input neural network. The main idea

Curriculum Learning	Data Aug.		MR All↓	MR Day↓	MR Night↓
	S	M			
Multimodal					
✓	✗	✗	9.1	9.19	8.93
✓	✓	✗	8.6	9.0	8.51
✓	✓	✓	8.54	8.92	8.47
✗	✓	✗	9.17	9.23	8.81
✗	✗	✓	9.03	9.18	8.87
✗	✓	✓	8.83	9.01	8.6
✓	✓	✓	8.31	8.64	8.0

TABLE II: Ablation study of different training strategies on KAIST dataset [40]. S and M stand for simple and mixup augmentation respectively.

λ_g	MR All↓	MR Day↓	MR Night↓
Multimodal			
0.1	8.42	8.86	8.2
0.3	8.31	8.64	8.0
0.7	8.19	8.30	7.76
1.0	8.07	8.16	7.51

TABLE III: Comparison of different loss balancing factors (λ_g) in Eqn. 6 on KAIST dataset[40]. MR is Miss Rate.

is to train using easier objects first and gradually increase the object’s difficulty level. It provided stable convergence to the global optimum. Mask and Predict [46] is a specific strategy in curriculum learning where the pedestrian box is progressively masked, and the network is expected to predict the boxes with the visible and masked regions. It was used to handle partially visible pedestrians due to occlusion. In this paper, we use the mask and predict-based curriculum learning defined in our previous work [47]. We mask the pedestrian regions with masking % increasing from 0% to 70% gradually over the training phases. As per Table II, we can observe that curriculum learning provides a significant improvement even on top of two data augmentation techniques. Our qualitative results show a good performance in occluded scenes and an improvement in generalization.

Data augmentation: Data augmentation is an essential ingredient of deep learning-based object detection algorithms to regularize the model. In this work, we apply the standard augmentation techniques such as random scaling of images between 0.8 to 1.2, image flipping with a probability of 0.3, enhancing contrast, adding Gaussian noise, and blur effect. We refer to these as simple augmentations (*S*). In addition to this, we use *mixup* [55], a data-agnostic augmentation technique that trains a network on pairs of examples and their labels based on convex combinations. *mixup* (*M*) can be represented as below.

$$\begin{aligned}\tilde{m} &= \omega m_i + (1 - \omega)m_j \\ \tilde{n} &= \omega n_i + (1 - \omega)n_j\end{aligned}\tag{9}$$

where m_i, m_j are raw input vectors and n_i, n_j are one-hot label encoding. (m_i, n_i) and (m_j, n_j) are two examples generated randomly from the training dataset and $\omega \in [0, 1]$. This technique is simple to implement and has low computa-

Methods	Multimodal (MR ↓)			Visible (MR ↓)			Thermal (MR ↓)		
	All	Day	Night	All	Day	Night	All	Day	Night
ACF [40]	31.34	29.59	34.98	32.01	29.85	36.77	31.90	30.40	34.81
Halfway Fusion [22]	25.75	24.88	26.59	25.10	24.29	26.12	25.51	25.20	24.90
Fusion RPN [48]	20.67	19.55	22.12	20.52	19.69	21.83	21.43	21.08	20.88
Fusion RPN+BF [48]	15.91	16.49	15.15	15.98	16.60	15.28	16.52	17.56	14.48
IAF R-CNN [26]	15.73	14.55	18.26	15.65	14.95	18.11	16.00	15.22	17.56
IATDNN+IASS [49]	14.95	14.67	15.72	15.14	14.82	15.87	15.08	15.02	15.20
RFA [50]	14.61	16.78	10.21	–	–	–	–	–	–
CIAN [51]	–	–	–	14.64	15.13	12.43	14.68	16.21	9.88
MSDS-RCNN [24]	11.63	10.60	13.73	11.28	9.91	14.21	12.51	12.02	13.01
CS-RCNN [52]	11.43	11.86	8.82	–	–	–	–	–	–
AR-CNN [28]	9.34	9.94	8.38	8.86	8.45	9.16	8.26	9.02	7.04
MBNet [29]	8.13	8.28	7.86	–	–	–	–	–	–
Ours	8.07	8.16	7.51	11.79	9.89	14.04	8.18	9.29	7.03

TABLE IV: Comparison of multimodal pedestrian detection on KAIST dataset [40] using Miss Rate (MR) metric.

Methods	mAP ↑
PiCA-Net [16]	65.80*
R ³ Net [16]	70.85*
tY [53]	63.00
SSTN101 [54]	73.22
Ours	78.03

TABLE V: Quantitative comparison of multimodal pedestrian detection on KAIST dataset [40] using mAP metric. (*) denotes the average of day and night mAP scores.

tional overhead. It provides regularization to noisy labels by generating mixed up patches. From Table II, it can be observed *mixup* provides an additional improvement on top of S with or without curriculum learning.

Loss balancing factor: The hyperparameter λ_g denotes the loss balancing factor between geometric loss (\mathcal{L}_g) and score map loss (\mathcal{L}_s) as shown in Equation 6. The range of this value is $[0, 1]$ and we heuristically test with different predefined values (0.1, 0.3, 0.7 and 1.0) of λ_g . MRs are reported in Table III showing that the optimal value of λ_g is 1.

C. Quantitative study

To facilitate a quantitative comparison with the state-of-the-art techniques, we evaluate our method on KAIST [40], CVC-14 [42] and UTokyo [43] multimodal datasets.

KAIST: Table IV compares the proposed method with other state-of-the-art approaches using Miss Rate (MR) metric for the day, night, and all scenarios. We achieve state-of-the-art results, but the improvement is incremental. Multimodal accuracy is also incremental over unimodal thermal accuracy; in fact, it degrades in night scenarios. As expected, visible unimodal performance is poor at night time and only slightly better at day time. We obtain the best thermal unimodal accuracy compared to other methods; however, we stood third in visible unimodal accuracy. As some of the recent works uses the more commonly used object detection metric, namely Mean Average Precision (mAP) score, we provide an additional comparative study in Table V. In this case, there is a large absolute improvement of 5% in accuracy.

UTokyo: Table VI compares the proposed method with other state-of-the-art multimodal approaches using the Miss

Methods	Miss Rate ↓
ACF+T+THOG [40]	59.77
Halfway Fusion [22]	39.80
MLF-CNN [56]	27.63
Ours	25.82

TABLE VI: Quantitative comparison of multimodal pedestrian detection on UTokyo dataset [43].

Methods	MR All ↓	MR Day ↓	MR Night ↓
MACF [57]	60.1	61.3	48.2
Choi et al. [58]	47.3	49.3	43.8
Halfway Fusion [57]	37.0	38.1	34.4
Park et al. [57]	31.4	31.8	30.8
AR-CNN [28]	22.1	24.7	18.1
MBNet [29]	21.1	24.7	13.5
Ours	19.04	20.32	12.86

TABLE VII: Quantitative comparison of pedestrian detection on CVC-14 dataset [42]. MR is Miss Rate.

Rate metric. The proposed method achieves an absolute improvement of roughly 2% relative to the previous state-of-the-art method [56].

CVC-14: Table VII compares the proposed method with other state-of-the-art multimodal approaches using the Miss Rate metric for the day, night, and all scenarios. It is to be noted that despite the alignment issue between color and thermal images due to improper camera calibration, the proposed approach outperformed other multimodal pedestrian detectors without performing any pre-processing or post-processing. An absolute improvement of 2% was obtained over the previous state-of-the-art method [29].

D. Qualitative study

Figures 3, 4 and 5 shows qualitative results of the proposed model on KAIST, CVC-14 and UTokyo dataset respectively. More qualitative results are provided in <https://youtu.be/FDJdSifuuCs>. Top and bottom rows of Figures 4 and 5 shows night and daytime scenes respectively. The proposed method provides accurate detection of pedestrians even in challenging scenarios. Small pedestrians are one such challenge, and good detection can be observed in Figure 5 where a small child (top left) and a far pedestrian (bottom

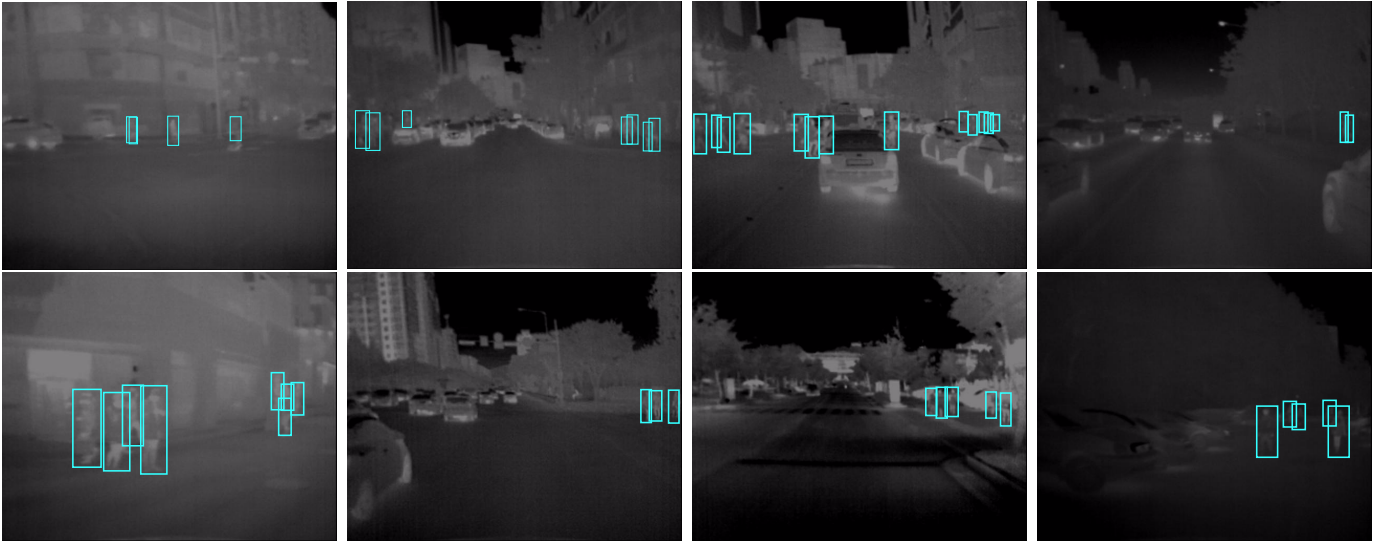


Fig. 3: Qualitative results of the proposed method on the KAIST [40] dataset.



Fig. 4: Qualitative results on the CVC-14 [42] dataset.



Fig. 5: Qualitative results on the UTokyo [43] dataset.

left) are detected accurately. Another challenging scenario is a crowded group of pedestrians with occlusions, and we can observe good detections in Figure 4. *SCoFA* module aids in learning context to provide robust detection in these scenarios. However, we occasionally observe a few missed detections in groups of pedestrians. In some cases, a group of pedestrians is detected as one pedestrian. Finally, partially visible or occluded pedestrians are detected well when there is sufficient visibility, as observed in the bottom right image of Figure 5.

Figure 6 compares the two unimodal outputs with multimodal model. The RGB image (left) fails to detect the pedestrian in the dark area marked by a green box in the first row. Both the thermal (middle) and multimodal (right) model can detect it successfully. Two pedestrians are missed in thermal image output in the second row but correctly detected in RGB and multimodal outputs. RGB image output produces a false positive marked by a red box in the third row, but it is not present in thermal and fusion outputs. These three scenarios illustrate that fusion can effectively combine both RGB and thermal inputs.

V. CONCLUSION

In this work, we have developed a novel end-to-end deep learning architecture for multimodal pedestrian detection. We have introduced the *Multimodal Feature Embedding Module* for the embedding of the two uni-modal encoder features into a lower-dimensional multimodal feature vector. It makes use of attention-guided graph networks to extract features representing the structural properties of pedestrians. We also introduced the *Spatio-Contextual Feature Aggregation Module*, which combines the spatial information obtained from its channel-wise attention block and the contextual information obtained from its 4Dir-IRNN block. We obtain state-of-the-art results on three public multimodal benchmarks, namely KAIST, CVC-14, and UTokyo datasets. We aim to extend our model to perform multimodal pedestrian action recognition to enable a more interactive autonomous driving system in future work.



Fig. 6: Comparison of unimodal and multimodal detections on KAIST dataset [40]. Yellow, blue & cyan colors are for the correct detections from RGB, thermal and both inputs respectively. Green & red bounding boxes indicate missed and false detections respectively.

REFERENCES

- [1] S. Kuutti, R. Bowden, Y. Jin, P. Barber, and S. Fallah, "A survey of deep learning applications to autonomous vehicle control," in *IEEE Transactions on Intelligent Transportation Systems*, vol. 22, 2020.
- [2] D. Gerónimo, A. M. López, A. D. Sappa, and T. Graf, "Survey of pedestrian detection for advanced driver assistance systems," in *IEEE Transactions on Pattern Analysis and Machine Intelligence*, vol. 32, no. 7, 2010, pp. 1239–1258.
- [3] M. Ye, Y. Cheng, X. Lan, and H. Zhu, "Improving night-time pedestrian retrieval with distribution alignment and contextual distance," in *IEEE Transactions on Industrial Informatics*, vol. 16, no. 1, 2020.
- [4] R. O. Chavez-Garcia and O. Aycard, "Multiple sensor fusion and classification for moving object detection and tracking," in *IEEE Transactions on Intelligent Transportation Systems*, vol. 17, no. 2, 2015, pp. 525–534.
- [5] D. Feng, C. Haase-Schuetz, L. Rosenbaum, H. Hertlein, C. Glaeser, F. Timm, W. Wiesbeck, and K. Dietmayer, "Deep multi-modal object detection and semantic segmentation for autonomous driving: Datasets, methods, and challenges," in *IEEE Transactions on Intelligent Transportation Systems*, vol. 22, 2020, pp. 1341–1360.
- [6] B. Miethig, A. Liu, S. Habibi, and M. v. Mohrenschildt, "Leveraging thermal imaging for autonomous driving," in *IEEE Transportation Electrification Conference and Expo*, 2019, pp. 1–5.
- [7] "Automotive night vision," https://en.wikipedia.org/wiki/Automotive_night_vision, Accessed May 14, 2021.
- [8] L. Yahiaoui, M. Uříčář, A. Das, and S. Yogamani, "Let the sunshine in: Sun glare detection on automotive surround-view cameras," in *Electronic Imaging. Society for Imaging Science and Technology*, 2020.
- [9] Y. Tian, P. Luo, X. Wang, and X. Tang, "Pedestrian detection aided by deep learning semantic tasks," in *IEEE Conference on Computer Vision and Pattern Recognition*, 2015, pp. 5079–5087.
- [10] W. Ouyang, X. Zeng, and X. Wang, "Learning mutual visibility relationship for pedestrian detection with a deep model," in *International booktitle of Computer Vision*, vol. 120, no. 1, 2016, pp. 14–27.
- [11] G. Brazil, X. Yin, and X. Liu, "Illuminating pedestrians via simultaneous detection & segmentation," in *IEEE International Conference on Computer Vision*, 2017, pp. 4950–4959.
- [12] L. Zhang, L. Lin, X. Liang, and K. He, "Is faster R-CNN doing well for pedestrian detection?" in *European Conference on Computer Vision*, 2016, pp. 443–457.
- [13] S. Ren, K. He, R. Girshick, and J. Sun, "Faster r-cnn: towards real-time object detection with region proposal networks," in *IEEE Transactions on Pattern Analysis and Machine Intelligence*, vol. 39, no. 6, 2016.
- [14] W. Liu, S. Liao, W. Ren, W. Hu, and Y. Yu, "High-level semantic feature detection: A new perspective for pedestrian detection," in *IEEE Conference on Computer Vision and Pattern Recognition*, 2019.
- [15] J. Baek, S. Hong, J. Kim, and E. Kim, "Efficient pedestrian detection at nighttime using a thermal camera," in *Sensors*, vol. 17, no. 8, 2017.
- [16] D. Ghose, S. M. Desai, S. Bhattacharya, D. Chakraborty, M. Fiterau, and T. Rahman, "Pedestrian detection in thermal images using saliency maps," in *IEEE Conference on Computer Vision and Pattern Recognition Workshops*, 2019.
- [17] C. Devaguptapu, N. Akolekar, M. M. Sharma, and V. N. Balasubramanian, "Borrow from anywhere: Pseudo multi-modal object detection in thermal imagery," in *IEEE Conference on Computer Vision and Pattern Recognition Workshops*, 2019.
- [18] J.-Y. Zhu, T. Park, P. Isola, and A. A. Efros, "Unpaired image-to-image translation using cycle-consistent adversarial networks," in *IEEE International Conference on Computer Vision*, 2017, pp. 2223–2232.
- [19] T. Guo, C. P. Huynh, and M. Solh, "Domain-adaptive pedestrian detection in thermal images," in *IEEE International Conference on Image Processing*, 2019, pp. 1660–1664.
- [20] M. Kieu, A. D. Bagdanov, M. Bertini, and A. Del Bimbo, "Task-conditioned domain adaptation for pedestrian detection in thermal imagery," in *European Conference on Computer Vision*, 2020.
- [21] J. Wagner, V. Fischer, M. Herman, and S. Behnke, "Multispectral pedestrian detection using deep fusion convolutional neural networks," in *ESANN*, vol. 587, 2016, pp. 509–514.
- [22] J. Liu, S. Zhang, S. Wang, and D. N. Metaxas, "Multispectral deep neural networks for pedestrian detection," in *27th British Machine Vision Conference*, 2016.
- [23] D. Xu, W. Ouyang, E. Ricci, X. Wang, and N. Sebe, "Learning cross-modal deep representations for robust pedestrian detection," in *IEEE Conference on Computer Vision and Pattern Recognition*, 2017, pp. 5363–5371.
- [24] C. Li, D. Song, R. Tong, and M. Tang, "Multispectral pedestrian detection via simultaneous detection and segmentation," in *British Machine Vision Conference 2018, BMVC 2018*. BMVA Press, 2018.
- [25] R. Yadav, A. Samir, H. Rashed, S. Yogamani, and R. Dahyot, "Cnn based color and thermal image fusion for object detection in automated driving," in *Irish Machine Vision and Image Processing*, 2020.
- [26] C. Li, D. Song, R. Tong, and M. Tang, "Illumination-aware faster r-cnn for robust multispectral pedestrian detection," in *Pattern Recognition*, vol. 85, 2019, pp. 161–171.
- [27] Y. Zheng, I. H. Izzat, and S. Ziaee, "Gfd-ssd: gated fusion double ssd for multispectral pedestrian detection," in *arXiv preprint:1903.06999*, 2019.
- [28] L. Zhang, X. Zhu, X. Chen, X. Yang, Z. Lei, and Z. Liu, "Weakly aligned cross-modal learning for multispectral pedestrian detection," in *IEEE International Conference on Computer Vision*, 2019.
- [29] K. Zhou, L. Chen, and X. Cao, "Improving multispectral pedestrian detection by addressing modality imbalance problems," in *European Conference on Computer Vision*, 2020.
- [30] J. Dai, H. Qi, Y. Xiong, Y. Li, G. Zhang, H. Hu, and Y. Wei, "Deformable convolutional networks," in *IEEE International Conference on Computer Vision*, 2017, pp. 764–773.
- [31] P. Veličković, G. Cucurull, A. Casanova, A. Romero, P. Liò, and Y. Bengio, "Graph Attention Networks," in *International Conference on Learning Representations*, 2018.
- [32] S. Bell, C. L. Zitnick, K. Bala, and R. Girshick, "Inside-outside net: Detecting objects in context with skip pooling and recurrent neural networks," in *IEEE Conference on Computer Vision and Pattern Recognition*, 2016, pp. 2874–2883.
- [33] S. Xie, R. Girshick, P. Dollár, Z. Tu, and K. He, "Aggregated residual transformations for deep neural networks," in *IEEE Conference on Computer Vision and Pattern Recognition*, 2017, pp. 1492–1500.
- [34] X. Zhou, C. Yao, H. Wen, Y. Wang, S. Zhou, W. He, and J. Liang, "East: an efficient and accurate scene text detector," in *IEEE Conference on Computer Vision and Pattern Recognition*, 2017, pp. 5551–5560.
- [35] V. R. Kumar, S. A. Hiremath, M. Bach, S. Milz, C. Witt, C. Pinard, S. Yogamani, and P. Mäder, "Fisheyedistancenet: Self-supervised scale-aware distance estimation using monocular fisheye camera for autonomous driving," in *2020 IEEE International Conference on Robotics and Automation (ICRA)*. IEEE, 2020.
- [36] H. Gao and S. Ji, "Graph u-nets," in *Proceedings of the 36th International Conference on Machine Learning, ICML 2019*, ser. Proceedings of Machine Learning Research, K. Chaudhuri and R. Salakhutdinov, Eds., vol. 97. PMLR, 2019, pp. 2083–2092.
- [37] W. Cai and Z. Wei, "Remote sensing image classification based on a cross-attention mechanism and graph convolution," *IEEE Geoscience and Remote Sensing Letters*, 2020.

- [38] L. Liu, Z. Qiu, G. Li, S. Liu, W. Ouyang, and L. Lin, "Crowd counting with deep structured scale integration network," in *IEEE International Conference on Computer Vision*, 2019, pp. 1774–1783.
- [39] K. He, X. Zhang, S. Ren, and J. Sun, "Deep residual learning for image recognition," in *IEEE Conference on Computer Vision and Pattern Recognition*, 2016, pp. 770–778.
- [40] S. Hwang, J. Park, N. Kim, Y. Choi, and I. S. Kweon, "Multispectral pedestrian detection: Benchmark dataset and baselines," in *IEEE Conference on Computer Vision and Pattern Recognition*, 2015, pp. 1037–1045.
- [41] S. Xie and Z. Tu, "Holistically-nested edge detection," in *IEEE International Conference on Computer Vision*, 2015, pp. 1395–1403.
- [42] A. González, Z. Fang, Y. Socarras, J. Serrat, D. Vázquez, J. Xu, and A. M. López, "Pedestrian detection at day/night time with visible and fir cameras: A comparison," in *Sensors*, vol. 16, no. 6. Multidisciplinary Digital Publishing Institute, 2016, p. 820.
- [43] K. Takumi, K. Watanabe, Q. Ha, A. Tejero-De-Pablos, Y. Ushiku, and T. Harada, "Multispectral object detection for autonomous vehicles," in *Thematic Workshops of ACM Multimedia 2017*, 2017, pp. 35–43.
- [44] P. Dollar, C. Wojek, B. Schiele, and P. Perona, "Pedestrian detection: An evaluation of the state of the art," in *IEEE transactions on pattern analysis and machine intelligence*, vol. 34, no. 4, 2011, pp. 743–761.
- [45] Y. Bengio, J. Louradour, R. Collobert, and J. Weston, "Curriculum learning," in *26th International Conference on Machine Learning*, 2009.
- [46] P. S. R. Kishore, S. Das, P. S. Mukherjee, and U. Bhattacharya, "Cluenet: A deep framework for occluded pedestrian pose estimation," in *British Machine Vision Conference*, 2019, p. 245.
- [47] S. Das, P. S. R. Kishore, and U. Bhattacharya, "An end-to-end framework for pose estimation of occluded pedestrians," in *IEEE International Conference on Image Processing*, 2020, pp. 1446–1450.
- [48] D. König, M. Adam, G. Jarvers, G. Layher, H. Neumann, and M. Teutsch, "Fully convolutional region proposal networks for multi-spectral person detection," in *IEEE Conference on Computer Vision and Pattern Recognition Workshops*, 2017, pp. 49–56.
- [49] D. Guan, Y. Cao, J. Yang, Y. Cao, and M. Y. Yang, "Fusion of multispectral data through illumination-aware deep neural networks for pedestrian detection," in *Information Fusion*, vol. 50, 2019, pp. 148–157.
- [50] L. Zhang, Z. Liu, X. Chen, and X. Yang, "The cross-modality disparity problem in multispectral pedestrian detection," in *arXiv preprint arXiv:1901.02645*, 2019.
- [51] L. Zhang, Z. Liu, S. Zhang, X. Yang, H. Qiao, K. Huang, and A. Husain, "Cross-modality interactive attention network for multispectral pedestrian detection," in *Information Fusion*, vol. 50. Elsevier, 2019.
- [52] Y. Zhang, Z. Yin, L. Nie, and S. Huang, "Attention based multi-layer fusion of multispectral images for pedestrian detection," in *IEEE Access*, vol. 8. IEEE, 2020, pp. 165 071–165 084.
- [53] M. Krišto, M. Ivasic-Kos, and M. Pobar, "Thermal object detection in difficult weather conditions using yolo," in *IEEE Access*, vol. 8, 2020.
- [54] F. Munir, S. Azam, and M. Jeon, "Sstn: Self-supervised domain adaptation thermal object detection for autonomous driving," in *arXiv preprint arXiv:2103.03150*, 2021.
- [55] H. Zhang, M. Cisse, Y. N. Dauphin, and D. Lopez-Paz, "mixup: Beyond empirical risk minimization," in *International Conference on Learning Representations*, 2018.
- [56] Y. Chen, H. Xie, and H. Shin, "Multi-layer fusion techniques using a cnn for multispectral pedestrian detection," in *IET Computer Vision*, vol. 12, no. 8, 2018, pp. 1179–1187.
- [57] K. Park, S. Kim, and K. Sohn, "Unified multi-spectral pedestrian detection based on probabilistic fusion networks," in *Pattern Recognition*, vol. 80, 2018, pp. 143–155.
- [58] H. Choi, S. Kim, K. Park, and K. Sohn, "Multi-spectral pedestrian detection based on accumulated object proposal with fully convolutional networks," in *23rd International Conference on Pattern Recognition*, 2016, pp. 621–626.



Kinjal Dasgupta received his B.Tech. degree in Electrical Engineering from the West Bengal University of Technology, India, in 2020. He is currently holding a Research Position at Indian Statistical Institute, Kolkata, India. His areas of current research interest are Scene Understanding and the relevant problems of Computer Vision related to Supervised/Unsupervised Learning, Domain Adaptation and Transfer Learning.



Arindam Das is a Lead Engineer in the department of Detection Vision Systems (DVS) at Valeo India. He is currently involved in deep learning based algorithm development activities for autonomous driving systems. He has nearly 8 years of industry experience in computer vision, deep learning & document analysis. He has authored 13 peer reviewed publications & 32 patents. His current area of research interest includes semi-supervised learning, domain adaptation & multispectral image analysis.



Sudip Das joined the Indian Statistical Institute in a research position of its Computer Vision and Pattern Recognition Unit at Kolkata after obtaining his B. Tech degree in Computer Science and Engineering from the West Bengal University of Technology (WBUT), India, in 2017. His principal area of research focuses on the relevant problems of Unsupervised Learning, Curriculum Learning, Transfer Learning and Domain Adaptation. He is also passionate to work on the various problems of autonomous driving. In particular, he did some research in Computer Vision, with the goal of Detecting, Segmenting and Pose Estimating of objects in Images or videos.



Ujjwal Bhattacharya is currently a member of the faculty of the Computer Vision and Pattern Recognition Unit of Indian Statistical Institute situated in Kolkata. He joined his current Institute in 1991 as a Junior Research Fellow after obtaining his M.Sc. and M. Phil. degrees in Pure Mathematics from Calcutta University. In the past, he collaborated with a few industries and research labs of India and abroad. In 1995, he received Young Scientist Award from the Indian Science Congress Association. Also, he received a few best paper awards from various groups. He is a senior member of the IEEE and a life member of IUPRAI, Indian unit of the IAPR. He has served as Program Committee member of various reputed International Conferences and Workshops. Also, he worked as a Co-Guest Editor of a few Special Issues of International Journals. His current research interests include machine learning, computer vision, image processing, document processing, handwriting recognition etc.



Senthil Yogamani is an Artificial Intelligence architect and holds a director level technical leader position at Valeo Ireland. He leads the research and design of AI algorithms for various modules of autonomous driving systems. He has over 14 years of experience in computer vision and machine learning including 12 years of experience in industrial automotive systems. He is an author of 100+ publications with 1700+ citations and 100+ inventions with 70 filed patent families. He serves on the editorial board of various leading IEEE automotive conferences including ITSC and IV. and advisory board of various industry consortia including Khronos, Cognitive Vehicles and IS Auto. He is a recipient of best associate editor award at ITSC 2015 and best paper award at ITST 2012.